- A Totally Synthetic, Self-Assembling, Adjuvant-Free MUC1 Glycopeptide Vaccine for Cancer Therapy
  Huang, Z.-H.; Shi, L.; Ma, J.-W.; Sun, Z.-Y.; Cai, H.; Chen, Y.-X.; Zhao, Y.-F.; Li, Y.-M. *J. Am. Chem. Soc.* **2012**, *134*, 8730–8733.
  Abstract:

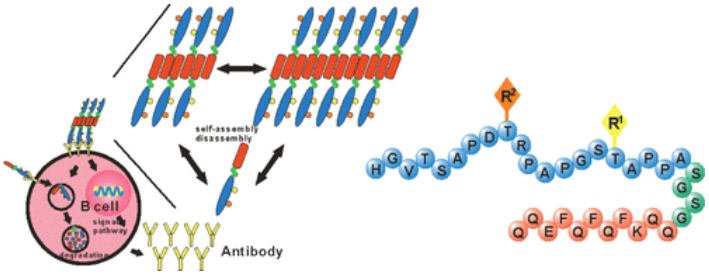

In the development of vaccines for epithelial tumors, the key targets are MUC1 proteins, which have a variable number of tandem repeats (VNTR) bearing tumor-associated carbohydrate antigens (TACAs), such as Tn and STn. A major obstacle in vaccine development is the low immunogenicity of the short MUC1 peptide. To overcome this obstacle, we designed, synthesized, and evaluated several totally synthetic self-adjuvanting vaccine candidates with self-assembly domains. These vaccine candidates aggregated into fibrils and displayed multivalent B-cell epitopes under mild conditions. Glycosylation of Tn antigen on the Thr residue of PDTRP sequence in MUC1 VNTR led to effective immune response. These vaccines elicited a high level antibody response without any adjuvant and induced antibodies that recognized human breast tumor cells. These vaccines appeared to act through a T-cell independent pathway and were associated with the activation of cytotoxic T cells. These fully synthetic, molecularly defined vaccine candidates had several features that hold promise for anticancer therapy.

- Conjugated Microporous Polymers as Molecular Sensing Devices: Microporous Architecture Enables Rapid Response and Enhances Sensitivity in Fluorescence-On and Fluorescence-Off Sensing
  Liu, X.; Xu, Y.; Jiang, D. *J. Am. Chem. Soc.* **2012**, *134*, 8738–8741.
  Abstract:

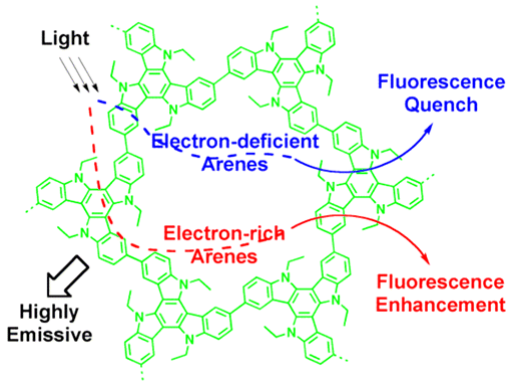

Conjugated polymers are attractive materials for the detection of chemicals because of their remarkable π-conjugation and photoluminescence properties. In this article, we report a new strategy for the construction of molecular detection systems with conjugated microporous polymers (CMPs). The condensation of a carbazole derivative, TCB, leads to the synthesis of a conjugated microporous polymer (TCB-CMP) that exhibits blue luminescence and possesses a large surface area. Compared with a linear polymer analogue, TCB-CMP showed enhanced detection sensitivity and

allowed for the rapid detection of arenes upon exposure to their vapors. TCB-CMP displayed prominent fluorescence enhancement in the presence of electron-rich arene vapors and drastic fluorescence quenching in the presence of electron-deficient arene vapors, and it could be reused without a loss of sensitivity and responsiveness. These characteristics are attributed to the microporous conjugated network of the material. Specifically, the micropores absorb arene molecules into the confined space of the polymer, the skeleton possesses a large surface area and provides a broad interface for arenes, and the network architecture facilitates exciton migration over the framework. These structural features function cooperatively, enhancing the signaling activity of TCB-CMP in fluorescence-on and fluorescence-off detection.

- Why the Mechanisms of Digermyne and Distannyne Reactions with H_2 Differ So Greatly
  Zhao, L.; Huang, F.; Lu, G.; Wang, Z.-X.; von Ragué Schleyer, P. *J. Am. Chem. Soc.* **2012**, *134*, 8856–8868.
  Abstract:

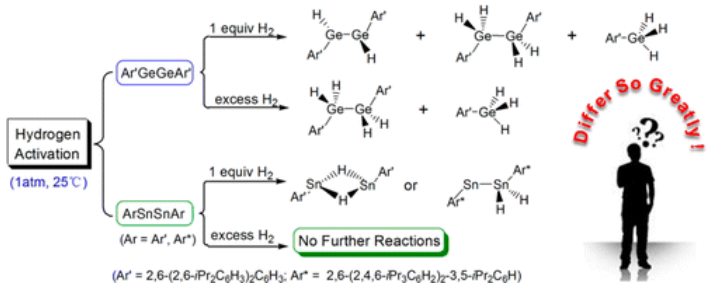

Despite their formal relationship to alkynes, Ar′GeGeAr′, Ar′SnSnAr′, and Ar*SnSnAr* [Ar′ = 2,6-(2,6-iPr$_2$C$_6$H$_3$)$_2$C$_6$H$_3$; Ar* = 2,6-(2,4,6-iPr$_3$C$_6$H$_2$)$_2$-3,5-iPr$_2$C$_6$H] exhibit high reactivity toward H_2, quite unlike acetylenes. Remarkably, the products are totally different. Ar′GeGeAr′ can react with 1–3 equiv of H_2 to give mixtures of Ar′HGeGeHAr′, Ar′H$_2$GeGeH$_2$Ar′, and Ar′GeH$_3$. In contrast, Ar′SnSnAr′ and Ar*SnSnAr* react with only 1 equiv of H_2 but give different types of products, Ar′Sn(μ-H)$_2$SnAr′ and Ar*SnSnH$_2$Ar*, respectively. In this work, this disparate behavior toward H_2 has been elucidated by TPSSTPSS DFT computations of the detailed reaction mechanisms, which provide insight into the different pathways involved. Ar′GeGeAr′ reacts with H_2 via three sequential steps: H_2 addition to Ar′GeGeAr′ to give singly H-bridged Ar′Ge(μ-H)GeHAr′; isomerization of the latter to the more reactive Ge(II) hydride Ar′GeGeH$_2$Ar′; and finally, addition of another H_2 to the hydride, either at a single Ge site, giving Ar′H$_2$GeGeH$_2$Ar′, or at a Ge–Ge joint site, affording Ar′GeH$_3$ + Ar′HGe:. Alternatively, Ar′Ge(μ-H)GeHAr′ also can isomerize into the kinetically stable Ar′HGeGeHAr′, which cannot react with H_2 directly but can be transformed to the reactive Ar′GeGeH$_2$Ar′. The activation of H_2 by Ar′SnSnAr′ is similar to that by Ar′GeGeAr′. The resulting singly H-bridged Ar′Sn(μ-H)SnHAr′ then isomerizes into Ar′HSnSnHAr′. The subsequent facile dissociation of the latter gives two Ar′HSn: species, which then reassemble into the experimental product Ar′Sn(μ-H)$_2$SnAr′. The reaction of Ar*SnSnAr* with H_2 forms in the kinetically and thermodynamically more stable Ar*SnSnH$_2$Ar* product rather than Ar*Sn(μ-H)$_2$SnAr*. The computed mechanisms successfully rationalize all of the known experimental differences among these reactions and yield the following insights into the behavior of the Ge and Sn species: (I) The active sites of Ar′EEAr′ (E = Ge, Sn) involve both E atoms, and the products with H_2 are the singly H-bridged Ar′E(μ-H)EHAr′ species rather than Ar′HEEHAr′ or Ar′EEH$_2$Ar′. (II) The heavier alkene congeners Ar′HEEHAr′ (E = Ge, Sn) cannot activate H_2 directly. Instead, Ar′HGeGeHAr′ must first isomerize into the more reactive Ar′GeGeH$_2$Ar′. Interestingly, the subsequent H_2 activation by Ar′GeGeH$_2$Ar′ can take place on either a single Ge site or a joint Ge–Ge

site, but Ar'SnSnH_2Ar' is not reactive toward H_2. The higher reactivity of Ar'GeGeH_2Ar' in comparison with Ar'SnSnH_2Ar' is due to the tendency of group 14 elements lower in the periodic table to have more stable lone pairs (i.e., the inert pair effect) and is responsible for the differences between the reactions of Ar'EEAr' (E = Ge, Sn) with H_2. Similarly, the carbene-like Ar'HGe: is more reactive toward H_2 than is Ar'HSn:. (III) The doubly H-bridged Ar'E(μ-H)$_2$EAr' (E = Ge, Sn) species are not reactive toward H_2.

- Paper-Based Blood Typing Device That Reports Patient's Blood Type "in Writing"
  Li, M.; Tian, J.; Al-Tamimi, M.; Shen, W. *Angew. Chem. Int. Ed.* **2012**, *51*, 5497-5501.
  Abstract:

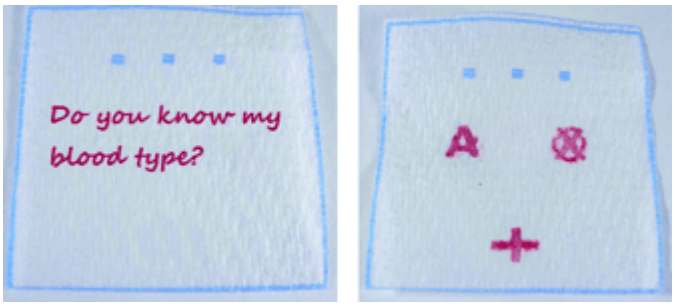

A response in writing: A low-cost bioactive paper device is designed to perform ABO and RhD blood typing tests, and the paper reports the results in writing. This idea was inspired by the vision of the British author, J. K. Rowling, through her novel "Harry Potter and the Chamber of Secrets" in which a piece of paper could be interrogated for information and unambiguous answers were received from the paper in writing.

- Amide-Forming Ligation of Acyltrifluoroborates and Hydroxylamines in Water
  Dumas, A. M.; Molander, G. A.; Bode, J. W. *Angew. Chem. Int. Ed.* **2012**, *51*, 5683-5686.
  Abstract:

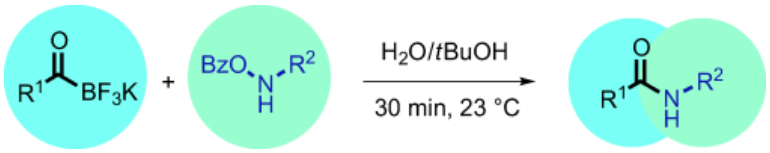

Come together, right now: Acyltrifluoroborates and O-benzoyl hydroxylamines come together to form amides in water (see scheme). The ligations are complete within minutes at room temperature and do not require any reagents or catalysts. The reaction has a broad substrate scope and tolerates unprotected functional groups.

- Granum-Like Stacking Structures with TiO_2–Graphene Nanosheets for Improving Photo-electric Conversion
  Yang, N.; Zhang, Y.; Halpert, J. E.; Zhai, J.; Wang, D.; Jiang, L. *Small* **2012**, *8*, 1762–1770.
  Abstract:

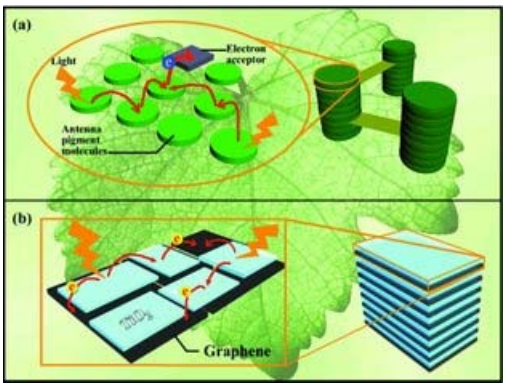

Solar energy is commonly considered to be one of the most important forms of future energy production. This is due to its ability to generate essentially free power, after installation, with low environmental impact. Green plants, meanwhile, exhibit a process for light-to-charge conversion that provides a useful model for using solar radiation efficiently. Granum, the core organ in photosynthesis consists of a stack of ~10–100 thylakoids containing pigments and electrons acceptors. Imitating the structure and function of granum, stacked structures are fabricated with TiO_2/graphene nanosheets as the thylakoids unit, and their photo-electric effect is studied by varying the number of layers present in the film. The photo-electric response of the graphene composites are found to be 20 times higher than that of pure TiO_2 in films with 25 units stacked. Importantly, the cathodic photocurrent changes to anodic photocurrent as the thickness increases, an important feature of efficient solar cells which is often ignored. Here graphene is proposed to perform similarly to the b6f complex in granum, by separating charges and transporting electrons through the stacked film. Using this innovation, stacked TiO_2/graphene structures are now able to significantly increase photoanode thickness in solar cells without losing the ability to conduct electrons.

- Functionalized Isothianaphthene Monomers That Promote Quinoidal Character in Donor–Acceptor
  Douglas, J. D.; Griffini, G.; Holcombe, T. W.; Young, E. P.; Lee, O. P. ; Chen, M. S. ; Fréchet, J.-M. *Macromolecules* **2012**, *45*, 4069–4074.
  Abstract:

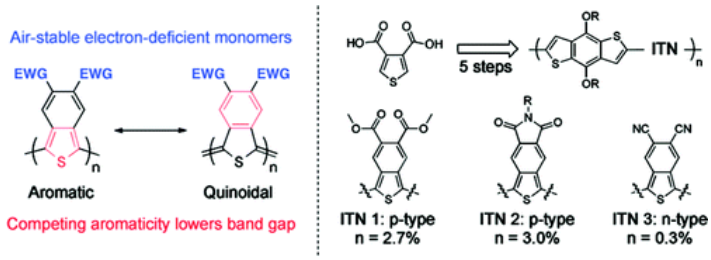

A series of low band gap isothianaphthene-based (ITN) polymers with various electron-withdrawing substituents and intrinsic quinoidal character were synthesized, characterized, and tested in organic photovoltaic (OPV) devices. The three investigated ITN cores contained either ester, imide, or nitrile functionalities and were each synthesized in only four linear steps. The relative electron-withdrawing strength of the three substituents on the ITN moiety was evaluated and correlated to the optical and electronic properties of ITN-based copolymers. The ester- and imide-containing p-type polymers reached device efficiencies as high as 3% in bulk heterojunction blends with phenyl C_{61}-butyric acid methyl ester ($PC_{61}BM$), while the significantly electron-deficient nitrile-functionalized polymer

behaved as an n-type material with an efficiency of 0.3% in bilayer devices with poly(3-(4-*n*-octyl)phenylthiophene) (POPT).

- Fullerene-Functionalized Donor–Acceptor Block Copolymers through Etherification as Stabilizers
  Heuken, M.; Komber, H.; Erdmann, T.; Senkovskyy, V.; Kiriy, A.; Voit, B. *Macromolecules* **2012**, *45*, 4101–4114.
  Abstract:

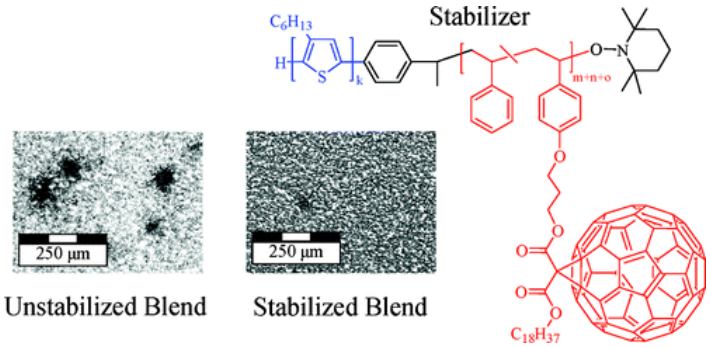

A new synthetic method for the covalent linking of fullerenes to polymers is introduced. The Bingel-reaction was used to prepare bromine-functionalized fullerene building blocks that could be covalently linked to hydroxyl groups of model copolymers by the cesium carbonate promoted Williamson ether synthesis. Subsequently, block copolymers with a second block based on styrene and hydroxystyrene or hydroxyethyl methacrylate could be synthesized with a poly(3-hexylthiophene)–TEMPO macroinitiator through NMRP. Fullerene derivatives were linked to these polymers in a controlled manner and donor–acceptor block copolymers with high fullerene contents of near 50 wt % were achieved.

- Multiphase design of autonomic self-healing thermoplastic elastomers
  Chen, Y.; Kushner, A. M.; Williams, G. A.; Guan, Z. *Nature Chem.* **2012**, *4*, 467–472.
  Abstract:

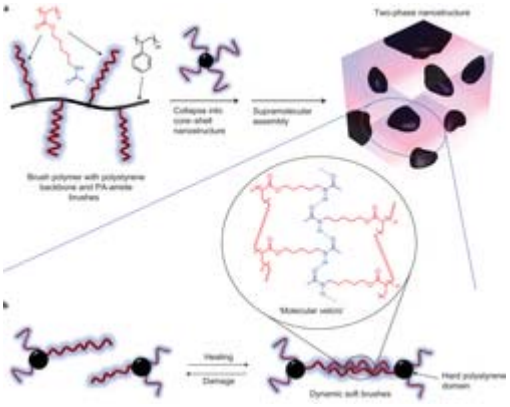

The development of polymers that can spontaneously repair themselves after mechanical damage would significantly improve the safety, lifetime, energy efficiency and environmental impact of man-made materials. Most approaches to self-healing materials require the input of external energy, healing agents, solvent or plasticizer. Despite intense research in this area, the synthesis of a stiff material with intrinsic self-healing ability remains a key challenge. Here, we show a design of multiphase supramolecular thermoplastic elastomers that combine high modulus and toughness with spontaneous healing capability. The designed hydrogen-bonding brush polymers self-assemble

into a hard–soft microphase-separated system, combining the enhanced stiffness and toughness of nanocomposites with the self-healing capability of dynamic supramolecular assemblies. In contrast to previous self-healing polymers, this new system spontaneously self-heals as a single-component solid material at ambient conditions, without the need for any external stimulus, healing agent, plasticizer or solvent.

- Logic gates based on ion transistors
  Tybrandt, K.; Forchheimer, R.; Berggren, M. *Nature Communications* **3**, Article number: 871.
  Abstract:

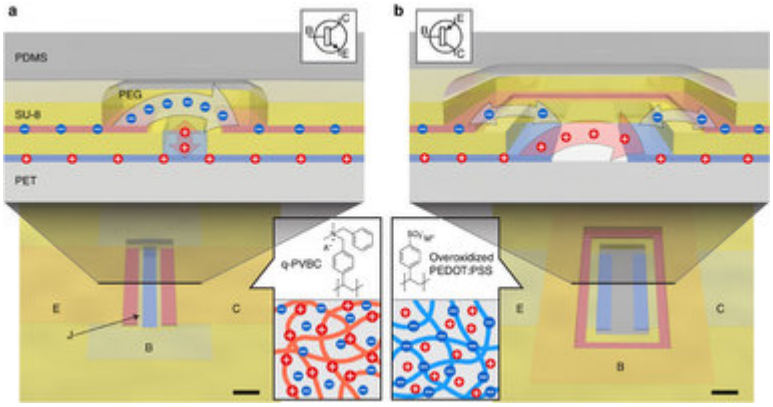

Precise control over processing, transport and delivery of ionic and molecular signals is of great importance in numerous fields of life sciences. Integrated circuits based on ion transistors would be one approach to route and dispense complex chemical signal patterns to achieve such control. To date several types of ion transistors have been reported; however, only individual devices have so far been presented and most of them are not functional at physiological salt concentrations. Here we report integrated chemical logic gates based on ion bipolar junction transistors. Inverters and NAND gates of both npn type and complementary type are demonstrated. We find that complementary ion gates have higher gain and lower power consumption, as compared with the single transistor-type gates, which imitates the advantages of complementary logics found in conventional electronics. Ion inverters and NAND gates lay the groundwork for further development of solid-state chemical delivery circuits.

- Shape-Programmed Folding of Stimuli-Responsive Polymer Bilayers
  Stoychev, G.; Zakharchenko, S.; Turcaud, S.; Dunlop, J. W. C.; Ionov, L. *ACS Nano* **2012**, *6*, 3925-3934.
  Abstract:

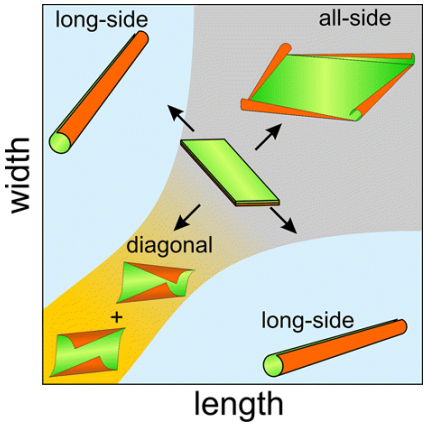

We investigated the folding of rectangular stimuli-responsive hydrogel-based polymer bilayers with different aspect ratios and relative thicknesses placed on a substrate. It was found that long-side rolling dominates at high aspect ratios (ratio of length to width) when the width is comparable to the circumference of the formed tubes, which corresponds to a small actuation strain. Rolling from all sides occurs for higher actuation, namely when the width and length considerably exceed the deformed circumference. In the case of moderate actuation, when both the width and length are comparable to the deformed circumference, diagonal rolling is observed. Short-side rolling was observed very rarely and in combination with diagonal rolling. On the basis of experimental observations, finite-element modeling and energetic considerations, we argued that bilayers placed on a substrate start to roll from corners due to quicker diffusion of water. Rolling from the long-side starts later but dominates at high aspect ratios, in agreement with energetic considerations. We have shown experimentally and by modeling that the main reasons causing a variety of rolling scenarios are (i) non-homogenous swelling due to the presence of the substrate and (ii) adhesion of the polymer to the substrate.

- Design of Patchy Particles Using Quaternary Self-Assembled Monolayers
  Pons-Siepermann, I. C.; Glotzer, S. C. *ACS Nano* **2012**, *6*, 3919-3924.
  Abstract:

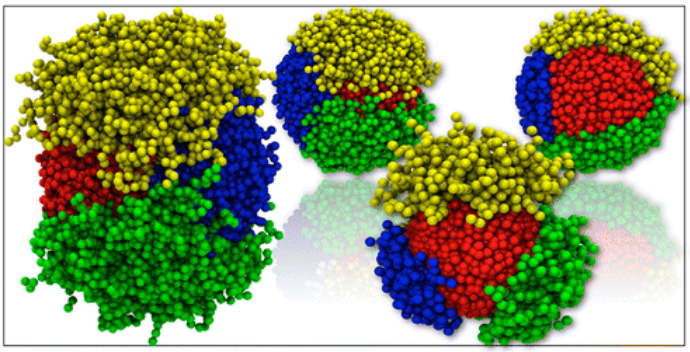

Binary and ternary self-assembled monolayers (SAMs) adsorbed on gold nanoparticles (NPs) have been previously studied for their propensity to form novel and unexpected patterns. The patterns found were shown to arise from a competition between immiscibilty of unlike surfactants and entropic gains due to length or other architectural differences between them. We investigate patterns self-assembled from quaternary monolayers on spherical nanoparticles. We perform simulations to study the effect of NP radius, degree of immiscibility between surfactants, length differences, and stoichiometry of the SAM on the formation of patterns. We report patterns analogous to binary and ternary cases, as well as some novel patterns specific to quaternary SAMs.

- Pattern Recognition of Cancer Cells Using Aptamer-Conjugated Magnetic Nanoparticles
  Bamrungsap, S.; Chen, T.; Shukoor, M. I.; Chen, Z.; Sefah, K.; Chen, Y.; Tan, W. *ACS Nano* **2012**, *6*, 3974-3981.
  Abstract:

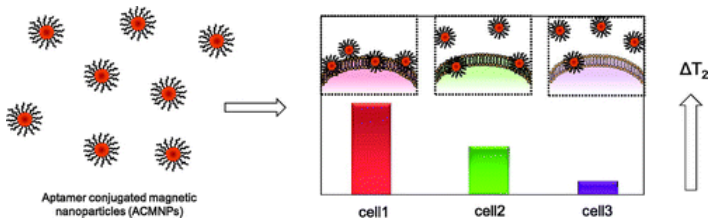

Biocompatible magnetic nanosensors based on reversible self-assembly of dispersed magnetic nanoparticles into stable nanoassemblies have been used as effective magnetic relaxation switches (MRSw) for the detection of molecular interactions. We report, for the first time, the design of MRSw based on aptamer-conjugated magnetic nanoparticles (ACMNPs). The ACMNPs capitalize on the ability of aptamers to specifically bind target cancer cells, as well as the large surface area of MNPs to accommodate multiple aptamer binding events. The ACMNPs can detect as few as 10 cancer cells in 250 µL of sample. The ACMNPs' specificity and sensitivity are also demonstrated by detection in cell mixtures and complex biological media, including fetal bovine serum, human plasma, and whole blood. Furthermore, by using an array of ACMNPs, various cell types can be differentiated through pattern recognition, thus creating a cellular molecular profile that will allow clinicians to accurately identify cancer cells at the molecular and single-cell level.

- Localization/Delocalization of Charges in Bay-Linked Perylene Bisimides
  Jiang, W.; Xiao, C.; Hao, L.; Wang, Z.; Ceymann, H.; Lambert, C.; Di Motta, S.; Negri, F. *Chem. Eur. J.* **2012**, *18*, 6764–6775.
  Abstract:

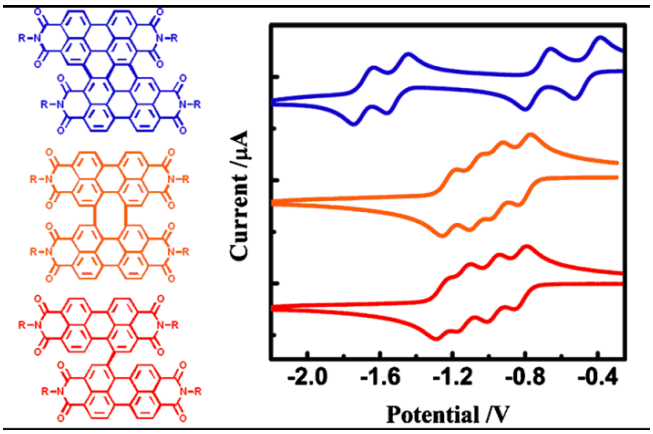

The copper-mediated Ullmann coupling of 1,7-dibromoperylene bisimides afforded structurally perfect singly-linked perylene bisimide (PBI) arrays, whilst the homo-coupling of 1,12-dibromoperylene bisimides gave doubly-linked and triply-linked diperylene bisimides. The interactions of three bay-linked diperylene bisimides that differed in their linkage (singly, doubly, and triply) were investigated in their neutral and reduced forms (mono-anion to tetra-anion). UV/Vis absorption and fluorescence spectroscopy revealed different degrees of interaction, which was explained by exciton coupling and conjugation effects. The electrochemical properties and spectroelectrochemistry also showed quite-different degrees of PBI interactions in the reduced mixed-valence species, which was apparent by the observation of CT bands. The interpretation of the experimental findings was supported by spin-restricted and -unrestricted DFT and time-dependent TD-DFT calculations with the long-range-corrected CAM-B3LYP functional. Accordingly, the degree of interaction in both the neutral and reduced forms of the bay-linked PBIs was qualitatively in the order doubly linked<singly linked≪triply linked, owing to the different degrees of twisting and flexibility between the two PBIs moieties. Only triply linked diPBI showed completely delocalized wavefunctions over the entire π-system.

- Supramolecular Assembly of Conjugated Polymers Containing Polyoxometalate Terminal Side Chains in Polar and Nonpolar Solvents

Yin, P.; Jin, L.; Li, D.; Cheng, P.; Vezenov, D. V.; Bitterlich, E.; Wu, X.; Peng, Z.; Liu, T. *Chem. Eur. J.* **2012**, *18*, 6754–6758.

Abstract:

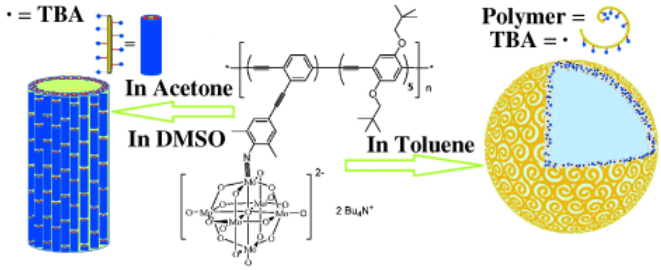

Clever combination: Three linear polymers containing polyoxometalate clusters on the side chains have been studied in both polar and nonpolar solvents. These polymers show amphiphilic properties in a nonpolar solvent (toluene) and form reverse vesicular supramolecular aggregates, while displaying polyelectrolyte properties in polar solvents and assembling into hollow tubelike structures (see scheme).

- Applications of dewetting in micro and nanotechnology
  Gentili, D.; Foschi, G.; Valle, F.; Cavallini, M.; Biscarini, F. *Chem. Soc. Rev.* **2012**, *41*, 4430-4443.
  Abstract:

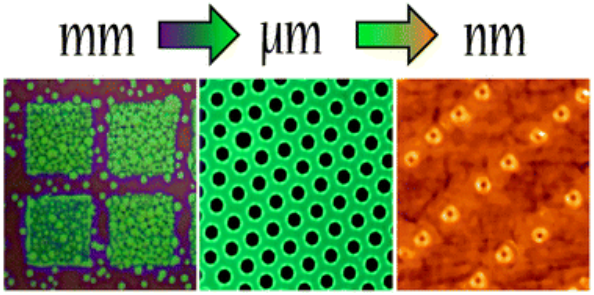

Dewetting is a spontaneous phenomenon where a thin film on a surface ruptures into an ensemble of separated objects, like droplets, stripes, and pillars. Spatial correlations with characteristic distance and object size emerge spontaneously across the whole dewetted area, leading to regular motifs with long-range order. Characteristic length scales depend on film thickness, which is a convenient and robust technological parameter. Dewetting is therefore an attractive paradigm for organizing a material into structures of well-defined micro- or nanometre-size, precisely positioned on a surface, thus avoiding lithographical processes. This *tutorial review* introduces the reader to the physical–chemical basis of dewetting, shows how the dewetting process can be applied to different functional materials with relevance in technological applications, and highlights the possible strategies to control the length scales of the dewetting process.

- Gold Nanoparticles in Chemical and Biological Sensing
  Saha, K.; Agasti, S. S.; Kim, C.; Li, X.; Rotello, V. M. *Chem. Rev.* **2012**, *112*, 2739–2779.
  Abstract:

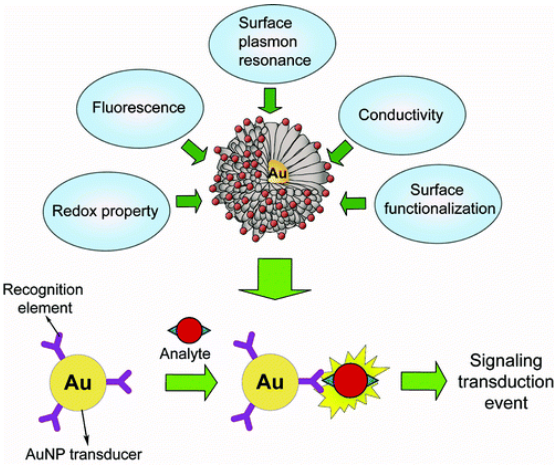

In this current review, we will highlight the several synthetic routes and properties of AuNPs that make them excellent probes for different sensing strategies. Furthermore, we will discuss various sensing strategies and major advances in the last two decades of research utilizing AuNPs in the detection of variety of target analytes including metal ions, organic molecules, proteins, nucleic acids, and microorganisms.

- "Click"-Functionalization of [60]Fullerene and Graphene with an Unsymmetrically Functionalized Diketopyrrolopyrrole (DPP) Derivative
  Castelaín, M.; Salavagione, H.; Segura, J. L. *Org. Lett.* **2012**, *14*, 2798-2801.
  Abstract:

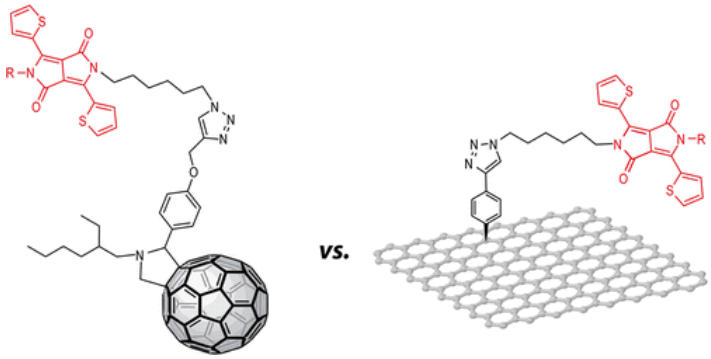

A synthetic strategy is developed that allows for the facile functionalization of carbon nanostructures thus providing the possibility of comparing the striking different optical and electrochemical properties of ensembles based on the diketopyrrolopyrrole (DPP) chromophore covalently attached to either [60]fullerene or graphene.

- Unprecedented "In Water" Imidazole Carbonylation: Paradigm Shift for Preparation of Urea and Carbamate
  Padiya, K. J.; Gavade, S.; Kardile, B.; Tiwari, M.; Bajare, S.; Mane, M.; Gaware, V.; Varghese, S.; Harel, D.; Kurhade, S. *Org. Lett.* **2012**, *14*, 2814-2817.
  Abstract:

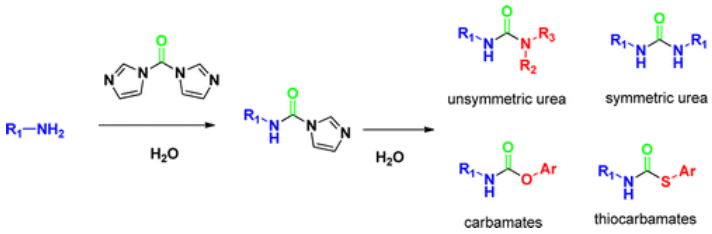

The first "In Water" imidazolecarbonylation of amine is described. A one pot reaction of carbonylimidazolide in water with a nucleophile provides an efficient and general method for the preparation of urea, carbamates and thiocarbamates. Use of an anhydrous solvent and an inert atmosphere could be avoided. Product precipitate out from the reaction mixture and can be obtained in high purity by filtration, resulting in a simple and scalable method.

- Tuning the Spectroscopic, Electrochemical, and Photovoltaic Properties of Triaryl Amine Based Sensitizers through Ring-Fused Thiophene Bridges
  Liu, Q.; Feng, Q.-Y.; Yamada, H.; Wang, Z.-S.; Ono, N.; You, X.-Z.; Shen, Z. *Chem. Asian J.* **2012**, *7*, 1312–1319.
  Abstract:

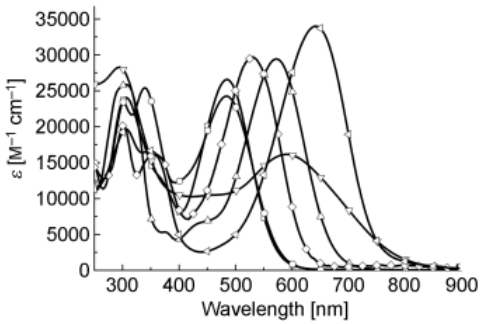

The ring-fused thiophene derivatives benzo[*c*]thiophene and its precursor bicyclo[2.2.2]octadiene (BCOD) have been introduced as π-conjugated spacers for organic push–pull sensitizers with dihexyloxy-substituted triphenylamine as donor and cyanoacrylic acid as acceptor (**OL1–OL6**). The effects of the fused ring on the spectroscopic and electrochemical properties of these sensitizers and their photovoltaic performance in dye-sensitized solar cells have been evaluated. Introduction of a binary benzo[*c*]thiophene and ethylenedioxy thiophene as π bridge caused a significant red shift of the characteristic intramolecular charge-transfer band to 642 nm. It is found that the sensitizer **OL3**, which contains one benzo[*c*]thiophene unit as π linker, gives the highest overall conversion efficiency of 5.03 % among all these dyes.

- Computational Design of Self-Assembling Protein Nanomaterials with Atomic Level Accuracy
  King, N. P.; Sheffler, W.; Sawaya, M. R.; Vollmar, B. S.; Sumida, J. P.; André, I.; Gonen, T.; Yeates, T. O.; Baker, D. *Science* **2012***, 336*, 1171-1175.
  Abstract:

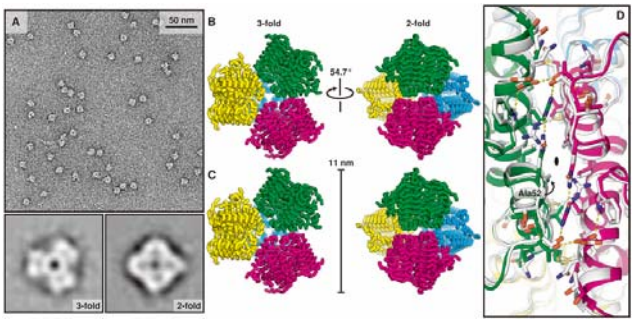

We describe a general computational method for designing proteins that self-assemble to a desired symmetric architecture. Protein building blocks are docked together symmetrically to identify complementary packing arrangements, and low-energy protein-protein interfaces are then designed between the building blocks in order to drive self-assembly. We used trimeric protein building blocks to design a 24-subunit, 13-nm diameter complex with octahedral symmetry and a 12-subunit, 11-nm diameter complex with tetrahedral symmetry. The designed proteins assembled to the desired oligomeric states in solution, and the crystal structures of the complexes revealed that the resulting materials closely match the design models. The method can be used to design a wide variety of self-assembling protein nanomaterials.

- Rocket Launcher Mechanism of Collaborative Actin Assembly Defined by Single-Molecule Imaging
  Breitsprecher, D.; Jaiswal, R.; Bombardier, J. P.; Gould, C. J.; Gelles, J.; Goode, B. L. *Science* **2012***, 336*, 1164-1169.
  Abstract:

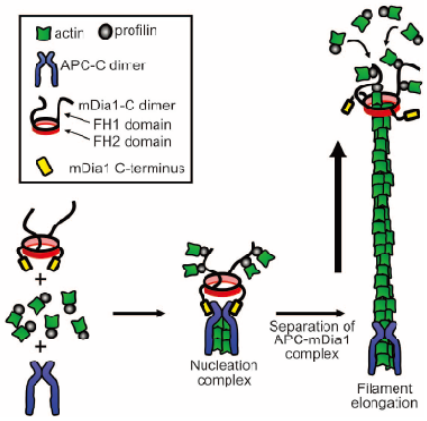

Interacting sets of actin assembly factors work together in cells, but the underlying mechanisms have remained obscure. We used triple-color single-molecule fluorescence microscopy to image the tumor suppressor adenomatous polyposis coli (APC) and the formin mDia1 during filament assembly. Complexes consisting of APC, mDia1, and actin monomers initiated actin filament formation, overcoming inhibition by capping protein and profilin. Upon filament polymerization, the complexes separated, with mDia1 moving processively on growing barbed ends while APC remained at the site of nucleation. Thus, the two assembly factors directly interact to initiate filament assembly and then separate but retain independent associations with either end of the growing filament.

- Designing Cell-Compatible Hydrogels for Biomedical Applications
  Seliktar, D. *Science* **2012,** *336*, 1124-1129.
  Abstract:

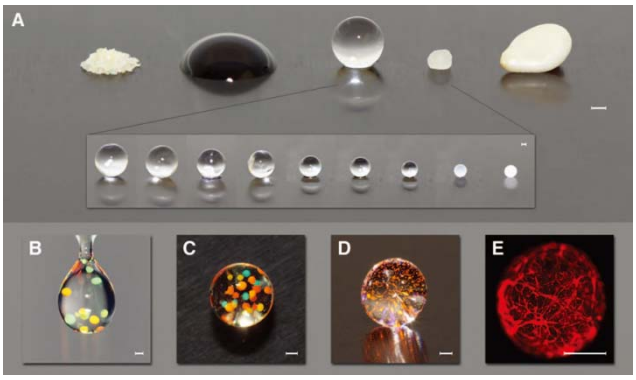

Hydrogels are polymeric materials distinguished by high water content and diverse physical properties. They can be engineered to resemble the extracellular environment of the body's tissues in ways that enable their use in medical implants, biosensors, and drug-delivery devices. Cell-compatible hydrogels are designed by using a strategy of coordinated control over physical properties and bioactivity to influence specific interactions with cellular systems, including spatial and temporal patterns of biochemical and biomechanical cues known to modulate cell behavior. Important new discoveries in stem cell research, cancer biology, and cellular morphogenesis have been realized with model hydrogel systems premised on these designs. Basic and clinical applications for hydrogels in cell therapy, tissue engineering, and biomedical research continue to drive design improvements using performance-based materials engineering paradigms.

- Complex shapes self-assembled from single-stranded DNA tiles.
  Wie, B.; Dai, M.; Yin, P. *Nature* **2012**, *485*, 623-626.
  Abstract:

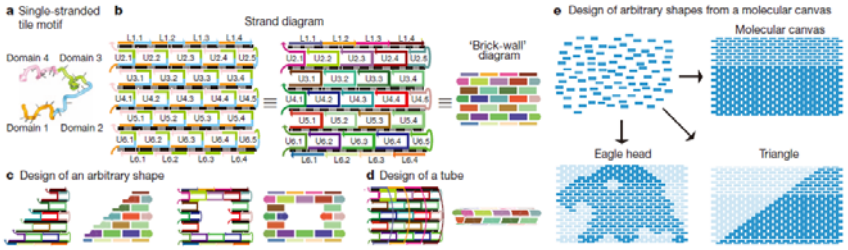

Programmed self-assembly of strands of nucleic acid has proved highly effective for creating a wide range of structures with desired shapes. A particularly successful implementation is DNA origami, in which a long scaffold strand is folded by hundreds of short auxiliary strands into a complex shape. Modular strategies are in principle simpler and more versatile and have been used to assemble DNA or RNA tiles into periodic and algorithmic two-dimensional lattices, extended ribbons and tubes three-dimensional crystals, polyhedra and simple finite two-dimensional shapes. But creating finite yet complex shapes from a large number of uniquely addressable tiles remains challenging. Here we solve this problem with the simplest tile form, a 'single-stranded tile' (SST) that consists of a 42-base strand of DNA composed entirely of concatenated sticky ends and that binds to four local neighbours during self-assembly. Although ribbons and tubes with controlled circumferences have been created using the SST approach, we extend it to assemble complex two-dimensional shapes and tubes from hundreds (in some cases more than one thousand) distinct tiles. Our main design feature is a self-assembled rectangle that serves as a molecular canvas, with each of its constituent SST strands-folded into a 3 nm-by-7nm tile and attached to four neighbouring tiles-acting as a pixel. A desired shape, drawn on the canvas, is then produced by one-pot annealing of all those strands that correspond to pixels covered by the target shape; the remaining strands are excluded. We

implement the strategy with a master strand collection that corresponds to a 310-pixel canvas, and then use appropriate strand subsets to construct 107 distinct and complex two-dimensional shapes, thereby establishing SST assembly as a simple, modular and robust framework for constructing nanostructures with prescribed shapes from short synthetic DNA strands.

- Fe^{2+} binds iron responsive element-RNA, selectively changing protein-binding affinities and regulating mRNA repression and activation
  Ma, J.; Haldar, S.; Khan, M. A.; Sharma, S. D.; Merrick, W. C.; Theil, E. C.; Goss, D. J. *Proc. Nat. Acad. Sci. USA* **2012***, 109*, 8417-8422.
  Abstract:

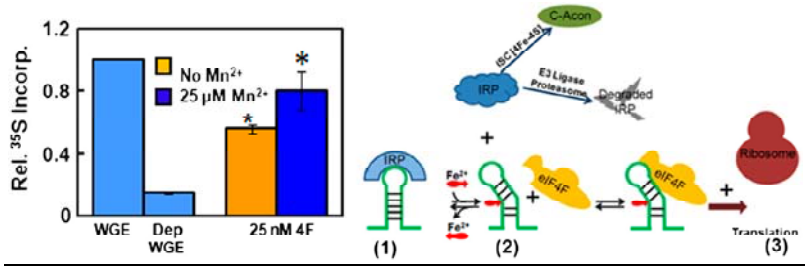

Iron increases synthesis rates of proteins encoded in iron-responsive element (IRE)-mRNAs; metabolic iron ("free," "labile") is Fe^{2+}. The noncoding IRE-RNA structure, approximately 30 nt, folds into a stem loop to control synthesis of proteins in iron trafficking, cell cycling, and nervous system function. IRE-RNA riboregulators bind specifically to iron-regulatory proteins (IRP) proteins, inhibiting ribosome binding. Deletion of the IRE-RNA from an mRNA decreases both IRP binding and IRP-independent protein synthesis, indicating effects of other "factors." Current models of IRE-mRNA regulation, emphasizing iron-dependent degradation/modification of IRP, lack answers about how iron increases IRE-RNA/IRP protein dissociation or how IRE-RNA, after IRP dissociation, influences protein synthesis rates. However, we observed Fe^{2+} (anaerobic) or Mn^{2+} selectively increase the IRE-RNA/IRP KD. Here we show: (i) Fe^{2+} binds to the IRE-RNA, altering its conformation (by 2-aminopurine fluorescence and ethidium bromide displacement); (ii) metal ions increase translation of IRE-mRNA in vitro; (iii) eukaryotic initiation factor (eIF)4F binds specifically with high affinity to IRE-RNA; (iv) Fe^{2+} increased eIF4F/IRE-RNA binding, which outcompetes IRP binding; (v) exogenous eIF4F rescued metal-dependent IRE-RNA translation in eIF4F-depeleted extracts. The regulation by metabolic iron binding to IRE-RNA to decrease inhibitor protein (IRP) binding and increase activator protein (eIF4F) binding identifies IRE-RNA as a riboregulator.

- Instant spectral assignment for advanced decision tree-driven mass spectrometry
  Bailey, D. J.; Rose, C. M.; McAlister, G. C.; Brumbaugh, J.; Yu, P.; Wenger, C. D.; Westphall, M. S.; Thomson, J. A.; Coon, J. J. *Proc. Nat. Acad. Sci. USA* **2012***, 109*, 8411-8416.
  Abstract:

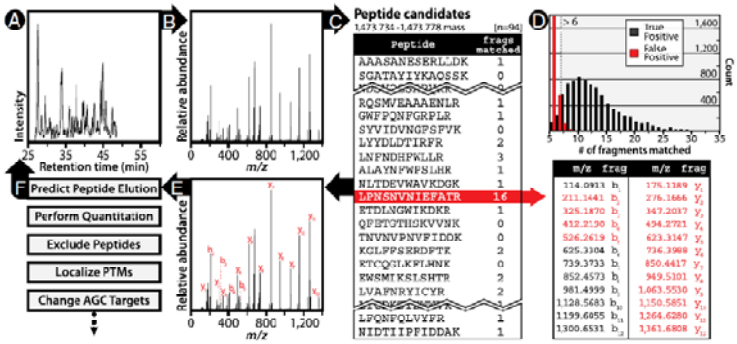

We have developed and implemented a sequence identification algorithm (*inSeq*) that processes tandem mass spectra in real-time using the mass spectrometer's (MS) onboard processors. The *inSeq* algorithmrelies on accurate mass tandemMS data for swift spectral matching with high accuracy. The instant spectral processing technology takes ~16 ms to execute and provides information to enable autonomous, real-time decision making by the MS system. Using *inSeq* and its advanced decision tree logic, we demonstrate (i) realtime prediction of peptide elution windows en masse (~3 min width, 3,000 targets), (ii) significant improvement of quantitative precision and accuracy (~3x boost in detected protein differences), and (iii) boosted rates of posttranslation modification site localization (90% agreement in real-time vs. offline localization rate and an approximate 25% gain in localized sites). The decision tree logic enabled by *inSeq* promises to circumvent problems with the conventional data-dependent acquisition paradigm and provides a direct route to streamlined and expedient targeted protein analysis.

- Lipid membranes in contact with aqueous phases of polymer solutions
  Dimova, R.; Lipowsky, R. *Soft Matter* **2012**, *8*, 2409-2415.
  Abstract:

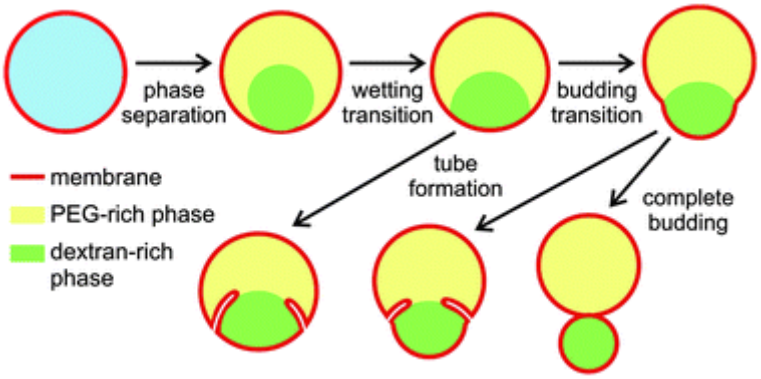

In this highlight, we describe recent developments in research on lipid vesicles encapsulating aqueous two-phase polymer solutions. Special emphasis is given on the morphological changes of the vesicles and the membrane transformations induced by the phase separation process, and on the interactions of the lipid bilayers with the phases. These interactions lead to a variety of interesting wetting phenomena and to the formation of membrane nanotubes. Future directions and possible developments in this research field are also discussed.

- Design and properties of supramolecular polymer gels
  Noro, A.; Hayashi, M.; Matsushita, Y. *Soft Matter* **2012**, *8*, 2416-2429.
  Abstract:

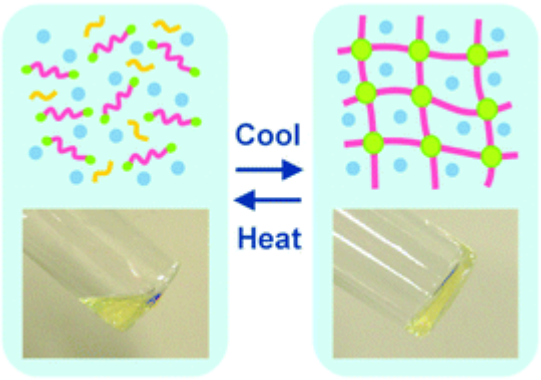

Supramolecular polymer gels are precisely designed physical gels brought together by reversible secondary interactions to form three dimensional networks of melt macromolecules. Generally, they differ from supramolecular gels because they are comprised of polymers instead of low molecular weight compounds. Recently, much effort has focused on designing supramolecular polymer gels and related materials with excellent properties; indeed, improvements have been made in their supramolecular interactions, complementarity in the non-covalent bonding units, the nature of the macromolecular building blocks, and strand elasticity of supramolecular polymer networks. Owing to the precise molecular design, they represent nanophase separation and characteristic viscoelasticity. Here, we review supramolecular polymer gels in terms of molecular design, morphology, and rheology. We also discuss future directions in practical application of supramolecular polymer gels.